



# Kinetic Study of Dry Reforming of Methane Over Ni–Ce/Al<sub>2</sub>O<sub>3</sub> Catalyst with Deactivation

Daniel Zambrano<sup>1</sup> · Jaime Soler<sup>1</sup> · Javier Herguido<sup>1</sup> · Miguel Menéndez<sup>1</sup>

Published online: 11 March 2019  
© Springer Science+Business Media, LLC, part of Springer Nature 2019

## Abstract

A kinetic study for dry reforming of methane over Ni–Ce/Al<sub>2</sub>O<sub>3</sub> catalyst was performed, taking into account both the main reactions and the catalyst deactivation. The catalyst was prepared by a sequential wet impregnation process, with loadings of 5 wt.% Ni and 10 wt.% Ce. Experimental tests were carried out in a fixed bed reactor between 475 and 550 °C and several spatial times, using nitrogen as diluent. Several kinetic equations were compared. The best fit of experimental data was achieved using a Langmuir–Hinshelwood mechanism which takes into account the presence of two active sites. Pre-exponential factor and activation energy were calculated. The kinetics of deactivation was also determined. The relationship between catalyst activity and coke concentration was also studied. Several deactivation equations were considered in order to choose the best fit with experimental data.

**Keywords** Catalyst deactivation · Kinetic modelling · Methane dry reforming · Hydrogen production

## 1 Introduction

Numerous efforts attempt to limit CO<sub>2</sub> and CH<sub>4</sub> emissions in order to minimize the global greenhouse warming. The production of synthesis gas via dry reforming of methane (1) is an attractive way to use CO<sub>2</sub> in the valorization of natural gas or to upgrade biogas obtained by anaerobic degradation of organic materials [1].



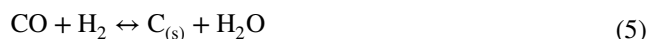
In addition to the main reaction, several (deleterious) side reactions may be involved in the process. The reverse of Water Gas Shift (WGS) (2), methane decomposition (3), the Boudouard reaction (4) and the carbon gasification reverse reaction (5) are the reactions with the greatest impact on the composition of the product gas.



**Electronic Supplementary Material** The online version of this article (<https://doi.org/10.1007/s11244-019-01157-2>) contains supplementary material, which is available to authorized users.

✉ Jaime Soler  
jsoler@unizar.es

<sup>1</sup> Department of Chemical and Environmental Engineering, Aragon Institute for Engineering Research (I3A), Universidad de Zaragoza, Zaragoza, Spain



Coke formation on the catalyst is one of the main disadvantages of this process and thus many researchers have aimed to obtain catalysts that would reduce the activity loss by coke. Reaction (3) is thermodynamically favored at high temperatures, while carbon generation is fostered at low temperatures in (4) and (5) [2].

An intense work focused on the development of catalysts capable of maintaining a good level of activity during a sufficiently long operating time, by decreasing coke formation rate [3]. Although catalysts based on noble metals such as Pd, Pt, Rh and Ru have been proposed [4, 5], their high price makes their industrial use unprofitable. Nickel catalysts present a good activity for this process [6, 7] as well as being economical. Other metals have been incorporated to reduce the coke formation, such as, for example, Ce [8] or Co [9]. The support used for these catalysts is usually alumina due to its low cost, high surface area and good mechanical properties. In particular, its resistance to attrition is a key need in a fluidized bed reactor.

Our group has found that the use of a two-zone fluidized bed reactor can counteract the catalyst deactivation, by

providing simultaneous reaction and regeneration in a single vessel [10]. In order to simulate this reactor and to search for the optimal operation conditions, a good knowledge of the process kinetics is needed, including also the catalyst deactivation kinetics.

Different kinetics for the dry methane reforming reaction have been published [11, 12]. The proposed reaction mechanisms depend on the catalyst studied. Reaction rate expressions are highly non-linear with respect to their parameters, particularly those models where the adsorption constants appear in both the numerator and the denominator of the expression.

The most common fittings are to Power-law, Eley–Rideal and Langmuir–Hinshelwood models [13]. The first one is the simplest but does not account for the reaction mechanisms.

The second one assumes that only the methane or CO<sub>2</sub> molecule is associatively adsorbed and the other one reacts from the gas phase. It assumes that rate-determining step is the reaction of the adsorbed species (CH<sub>4</sub> or CO<sub>2</sub>) with the gas phase one to yield products. However, Langmuir–Hinshelwood kinetic models are the result of reaction mechanisms which imply adsorption of the reactants and a later rate-determining surface reaction of these species to products.

The Langmuir–Hinshelwood model supposes that one reaction step is slow enough to become rate limiting while the other ones are in thermodynamic equilibrium. This last model has been used more frequently for nickel-based catalysts because it provides a more-realistic reaction kinetic model of comparable fitting quality especially in the low temperature range of  $T < 720$  °C. Methane decomposition reaction controls at higher reaction temperature regime [14]. We have reviewed mechanistical models for the reaction kinetic in literature finding out that only one of them [15] takes into account simultaneously reactions (1) and (2) and catalyst deactivation.

Therefore, the objective of this work is to obtain a kinetic model of both reaction and deactivation with the Ni–Ce/Al<sub>2</sub>O<sub>3</sub> catalyst and to obtain a relationship between the catalyst activity and the amount of coke deposited.

## 2 Experimental Section

### 2.1 Catalyst Preparation

A Ni–Ce/Al<sub>2</sub>O<sub>3</sub> catalyst was synthesized in our lab. The metals were added by the incipient wetness method. First, the Al<sub>2</sub>O<sub>3</sub> support (Sasol, Puralox®SCCa-150/200) was sieved to a size between 106 and 180 μm, and calcined in a muffle furnace (Nabertherm, B180) with a heating rate of 1°C/min until 950 °C, keeping this temperature for 1 h. The support was then impregnated with a solution of Ce(NO<sub>3</sub>)<sub>3</sub>·6H<sub>2</sub>O

(Sigma Aldrich, 99.999 wt.%) with an appropriate concentration to achieve the desired metal load. The resulting product was dried at 120 °C for 24 h and calcined at 950 °C for 1 h. The procedure was repeated with a second solution of nickel nitrate (Ni(NO<sub>3</sub>)<sub>2</sub>·6H<sub>2</sub>O, Sigma Aldrich, 99.999 wt.%). Finally, the product was dried and calcined, applying the same procedure as with the first precursor.

### 2.2 Reactor Setup

The catalytic experiments were carried out in a fixed-bed quartz reactor (1 cm i.d.), for which a laboratory-scale plant was assembled. Gaseous species were analyzed on-line by gas chromatography and coke formation was determined by carbon balance and by combustion with oxygen. Previous studies were carried out to ensure that the reaction rate was completely controlled by the intrinsic kinetics, thus avoiding mass transfer effects.

### 2.3 Fixed Bed Reactor Tests

Several series of experiments were carried out in a fixed bed reactor. Reactant fed was varied, using nitrogen as diluent, from a CH<sub>4</sub>:CO<sub>2</sub>:N<sub>2</sub> molar ratio 1:0.6:0.4 to 1:1.6:0.6, temperatures between 475 °C and 550 °C and space times ( $W/F_{\text{CH}_4}$ ) between 0.5 and 2.0 g<sub>cat</sub> h mol<sup>-1</sup> were employed. Exhaust gases were analyzed every 20 min during 4 h. Table 1 presents the employed operating conditions.

Diffusional control studies were carried out in order to find the maximum values of particle size, as well as the minimum flow rate, at which the reaction is controlled only by the kinetics, i.e. the observed reaction rate is not affected by mass transfer.

First, we performed experiments with different particle sizes (catalyst). We found out that with particle sizes larger than around 180 μm conversions were not reproducible. On the other hand, with very small particles (sizes lower than around 100 μm) too high pressure gradients were generated inside the reactor ( $\Delta P \geq 0.2$  bar). Therefore, the most suitable catalyst size was 106–180 μm. The conversion values

**Table 1** Operating conditions

T (°C)	CH <sub>4</sub> :CO <sub>2</sub> :N <sub>2</sub>	W/F <sub>CH<sub>4</sub>o</sub> (g <sub>cat</sub> mol <sup>-1</sup> h)
475	1:1:0.5	0.5   0.7   1.0   1.5   2.0
500	1:1:0.5	0.5   0.7   1.0   1.5   2.0
525	1:1:0.5	0.5   0.7   1.0   1.5   2.0
	1:1:0.0	0.4   0.6   0.8   1.2   1.6
	1:1:1.3	0.6   1.0   1.3   2.0   2.6
	1:0.6:0.4	0.4   0.6   0.8   1.2   1.6
	1:1.6:0.6	0.6   1.0   1.3   2.0   2.6
550	1:1:0.5	0.5   0.7   1.0   1.5   2.0

and operating conditions for these experiments are given in Supplementary information section.

Later, experiments were conducted operating with the same spatial time ( $W/F_{\text{CH}_4} = 2.2 \text{ g}_{\text{cat}} \text{ h mol}^{-1}$ ) but with different feed flow rates, in order to determine the minimum flow rate to prevent the external mass transfer from acting as the limiting step. Results are given in the Supplementary information section.

Methane and  $\text{CO}_2$  conversion and yield to gaseous product were defined as follows.

$$X_{\text{CH}_4} = \frac{[\text{F}_{\text{CH}_4}]_{\text{in}} - [\text{F}_{\text{CH}_4}]_{\text{out}}}{[\text{F}_{\text{CH}_4}]_{\text{in}}} \times 100 \quad (6)$$

$$X_{\text{CO}_2} = \frac{[\text{F}_{\text{CO}_2}]_{\text{in}} - [\text{F}_{\text{CO}_2}]_{\text{out}}}{[\text{F}_{\text{CO}_2}]_{\text{in}}} \times 100 \quad (7)$$

$$Y_{\text{CO}} = \frac{[\text{F}_{\text{CO}}]_{\text{out}}}{[\text{F}_{\text{CH}_4}]_{\text{in}} - [\text{F}_{\text{CO}_2}]_{\text{in}}} \times 100 \quad (8)$$

$$Y_{\text{H}_2} = \frac{[\text{F}_{\text{H}_2}]_{\text{out}}}{2[\text{F}_{\text{CH}_4}]_{\text{in}}} \times 100 \quad (9)$$

$$\text{H}_2/\text{CO} = \frac{[\text{F}_{\text{H}_2}]_{\text{out}}}{[\text{F}_{\text{CO}}]_{\text{out}}} \times 100 \quad (10)$$

After each experiment, the catalyst was regenerated at 600 °C with a stream of diluted  $\text{O}_2$  (2% in nitrogen) to remove the formed coke. Throughout the reduction process the carbon oxides content in the exit gas was analysed to estimate the coke amount in the spent catalysts. Then it was reduced for 3 h in a stream of  $\text{H}_2$  at 700 °C for its activation, before the next experiment.

Instantaneous water and coke yields were calculated by mass balance. The total carbon balance, when the coke measured during the catalyst regeneration was included, was  $99 \pm 0.5\%$ . A list with the results for every operational condition is provided in the Supplementary information section.

## 2.4 Modelling

Several programs developed in MatLab® were used to fit the kinetic models to the experimental data. The programs perform the fitting by numerically integrating the design equation of the plug flow reactor applied to each gaseous specie and minimizing the sum of squared residuals. The routines for resolution of ODEs and global optimization from Matlab Toolboxes were employed.

The discrimination and selection of models were made based on statistical criteria of model selection, such as the Akaike Information Criterion (AIC), the Bayesian Information Criterion (BIC) and the Fisher's F Test. The calculation of these criteria, and of the indicators for the goodness of fit for each model, was included within the above programs. In addition, we checked that the models were thermodynamically consistent. More details about the model comparison criteria are provided in the Supplementary information section.

An extensive bibliographical review was made by compiling several kinetic models proposed in previous works for the dry methane reforming, mostly on nickel catalysts. The following models, taken from literature, were compared (Supporting information section, Tables S41–S44): Basic model, Eley–Rideal (ER) [16, 17], Stepwise (SW) [18] and Langmuir–Hinshelwood [19–23] (LH). For the dry reforming reaction (1) a total of 13 mechanistic-type models obtained from the literature (i.e. [24–26]) were considered. The secondary reaction (2) was studied in other works [27, 28] not devoted to dry reforming of methane or was supposed to be in chemical equilibrium [11, 14]. Commonly, reactions (3), (4) and (5) were not taken into account in the kinetic models, but some authors have added the rate equations corresponding to these reactions [29–31].

As we will describe in more detail in the next section, the kinetic modelling of the reactions was performed in several steps:

- Starting kinetic model for the initial reaction rate. In this step the experimental data were extrapolated to zero time, where the catalyst is fully active. These initial values of molar flow for each species (i.e.,  $[F_i]_{\text{out}}$  at  $t=0$ ) were employed to obtain the equations describing the kinetics at zero time.
- Kinetic modelling of deactivation. Using the kinetics obtained from the initial reaction rate, the deactivation equation that best fitted the change of product distribution along time-on-stream was obtained.
- Refinement of the values for the kinetic constants, using all the experimental data, with the equations obtained in the previous steps and using the previously obtained kinetic constants as initial values.

In addition, since it will be necessary for the reactor design, a relationship between activity and coke content was developed, based on the mechanistic model previously selected.

As aforementioned, to obtain the values of reaction rate without deactivation the experimental results were extrapolated to zero time. For the kinetic modelling, reactions 1 and 2 were considered as the reactions that generate and consume part of the product respectively, while the reactions

**Table 2** Rate models expressions for methane dry reforming

No	Rate Model	Reference
LH1	$r_1 = \frac{k_1 K_{CH_4} K_{CO_2} P_{CH_4} P_{CO_2}}{(1 + K_{CH_4} P_{CH_4} + K_{CO_2} P_{CO_2})^2} \left( 1 - \frac{P_{CO}^2 P_{H_2}}{P_{CH_4} P_{CO_2} K_{eq1}} \right)$	[11, 12, 14, 15, 17, 19–22]
LH2	$r_1 = \frac{k_1 K_{CH_4} P_{CH_4} \sqrt{K_{CO_2} P_{CO_2}}}{(1 + K_{CH_4} P_{CH_4} + \sqrt{K_{CO_2} P_{CO_2}})^2} \left( 1 - \frac{P_{CO}^2 P_{H_2}}{P_{CH_4} P_{CO_2} K_{eq1}} \right)$	[19]
LH3	$r_1 = \frac{k_1 K_{CO_2} P_{CO_2} \sqrt{K_{CH_4} P_{CH_4}}}{(1 + \sqrt{K_{CH_4} P_{CH_4}})(1 + K_{CO_2} P_{CO_2})} \left( 1 - \frac{P_{CO}^2 P_{H_2}}{P_{CH_4} P_{CO_2} K_{eq1}} \right)$	[19]
LH4	$r_1 = \frac{k_1 \sqrt{K_{CH_4} P_{CH_4} K_{CO_2} P_{CO_2}}}{(1 + \sqrt{K_{CH_4} P_{CH_4}} + \sqrt{K_{CO_2} P_{CO_2}})^2} \left( 1 - \frac{P_{CO}^2 P_{H_2}}{P_{CH_4} P_{CO_2} K_{eq1}} \right)$	[19, 24]

**Table 3** Catalyst deactivation models compared

Id.	Model
LDKM	$-\frac{da}{dt} = \varphi_d a^d$
DMRA 1	$-\frac{da}{dt} = \varphi_d a^d - \varphi_r$
DMRA 2	$-\frac{da}{dt} = \varphi_d a^d - \varphi_r a^{dm}$
DMRA 3	$-\frac{da}{dt} = \varphi_d a^{m-1/m} (a^{1/m} - a_s^{1/m})^h$
DMRA 4	$-\frac{da}{dt} = \varphi_d a^d - \varphi_r a^{dm} + \varphi_r a$

Where  $\varphi_d$  is the deactivation function,  $\varphi_r$  is the regeneration function,  $a$  is the activity,  $m$  and  $h$  are the number of active sites involved in the rate determining step of the main reaction and of coke formation, respectively, as is the residual activity,  $d = \frac{m+h-1}{m}, d_m = \frac{m-1}{m}$

3, 4 and 5 generate or gasify coke depending on the gas phase composition. Due to the uncertainty of the number of secondary reactions that actually occur in the process, different simulation scenarios (SC) were proposed, considering from 2 to 5 simultaneous reactions. The scenario with the reactions (1), (2) and (3) was the one that presented the best results.

All the models considered in the fit of reaction rate at zero-time, for both the main reaction and the secondary ones, are detailed in Supplementary Information. Table 2 presents the equations for LH type models that offered the best fit to the experimental data.

We have not found previous studies on the kinetic modelling of catalyst deactivation by coke in dry methane reforming. The only one previous study on the kinetic modelling

catalyst deactivation by coke in dry methane reforming, that kinetic model was developed for Ni–Co/Al<sub>2</sub>O<sub>3</sub>, while Ni–Ce/Al<sub>2</sub>O<sub>3</sub> is known to be more stable. In addition, that kinetic model does not account for the influence of the operating conditions on the deactivation constant. We considered for the catalyst deactivation the kinetic deactivation model of Levenspiel (LDKM) [32] and the models of deactivation with residual activity (DMRA) [33]. Table 3 summarizes the equations used in the kinetic modelling of catalyst deactivation. Deactivation models are explained in detail in the Supplementary information section (Table S45), taking into account the number of active sites involved in the rate determining step of the main reaction and of the coke formation.

### 3 Results and Discussion

#### 3.1 Zero-Time Data Fitting

The modelling of the reaction kinetics at zero time was carried out by comparing models proposed in different scenarios. A first approximation (SC1) was made by considering only reactions (1) and (2). Different models from literature were considered for reaction (1), while a basic power-law model was adopted for reaction (2). Reaction (2) was considered as a non-equilibrium reaction, because such behaviour was observed in some of our experimental data. According to this first approximation we concluded that the type of model that best fit the experimental data were the Langmuir–Hinshelwood one for 1 (Table 2). LH1 is the best model according to statistical criteria (AIC, BIC, F).

The second scenario (SC2) considered all the models collected from the bibliography for 1 reaction and a LH type model for reaction (2) [27, 28]. Again, LH1 model provided the best fit to the experimental data and, additionally, an improvement was found in the adjustment with respect to the first approximation (Table 4). This means that the LH model describes the reaction 2 better than the power law type model.

Once the models for reaction 1 and 2 were set, several other scenarios were considered, where the participation of reactions 3, 4 and 5 was considered, either forward (forming coke) or backward (gasifying coke). Most of these results were discarded since some constants were not significantly different from zero or because the lack of physical sense (for

**Table 4** Zero-time kinetic model (SC2)

Model	R <sup>2</sup>	AR <sup>2</sup>	SSE	AIC	BIC	F
LH1	0.67	0.66	0.040	–1219	–7.99	17,043
LH2	0.65	0.63	0.043	–1208	–7.92	16,371
LH3	0.64	0.62	0.044	–1205	–7.89	16,079
LH4	0.64	0.62	0.044	–1204	–7.89	15,988

example, negative activation energies). However, there was a scenario (SC3) that presented kinetic constants reliable enough: this was the scenario that considered the reactions 1, 2 and the reaction 3 as a coke former. The experimental results were fit by firstly considering a power law model for reaction 3, and then considering a LH type model obtained from the literature [27, 29]. Table 5 presents the statistical criteria comparing models for the three scenarios with the highest data reliability.

Therefore, the scenario that best fits the data is scenario 3 (SC3) which considers three reactions (1, 2 and 3). In addition, the models selected for these three reactions are LH-type models, which consider the participation of two active sites in the rate determining step. So, scenario 3 will be used from now on. Another important aspect to take into account is the use of the same adsorption constant ( $K_{\text{CH}_4}$ ,  $K_{\text{CO}_2}$ ,  $K_{\text{H}_2}$ ) for the three reactions. Some researchers consider different adsorption constants for each reaction, giving greater freedom to the data fitting, but achieving kinetic equations with less mechanistic meaning.

An example of  $\text{CH}_4$  and  $\text{CO}_2$  conversion and  $\text{CO}$  and  $\text{H}_2$  yield evolution with space time and different fed compositions, is shown in Fig. 1. A good fit of the selected model to the experimental data can be seen. The influence of temperature is shown in Fig. 2. Again, a good fit between model and experimental data is observed. As could be expected, the higher the temperature the higher are the  $\text{CH}_4$  conversion and  $\text{H}_2$  yield, which is consistent with other works [34]. The  $\text{H}_2/\text{CO}$  molar ratio is presented in Fig. 3. The obtained values are lower than unity, which suggests the occurrence of side reactions (2) in addition to the main reaction (1). Moreover, this ratio slightly increases with temperature and space time up to  $1 \text{ g}_{\text{cat}} \text{ h mol}^{-1}$ . Above this value, the behavior remains stable. Parity plot is presented in Fig. 4. It can be seen that all results are between the  $\pm 15\%$  lines.

### 3.2 Deactivation Fitting

The catalyst deactivation modeling was carried out by integrating the differential equations presented in Table 3, considering only the physically more probable cases, i.e. with values of 1 or 2 for the coefficients  $m$  and  $h$  (number of active sites involved in the rate determining step of the main reaction and of the coke formation, respectively). In addition, from the zero-time kinetic modeling, according

to the reaction mechanism of the selected model (LH1) for reaction 1, there are two active sites involved in the rate determining step. Taking this into consideration, the coefficient  $m$  should be 2. Thus, taking values of 1 and 2 for the parameter  $h$ , the resulting different deactivation models were tested. Having fixed the values of  $m$  and  $h$ , the kinetic parameters in functions  $\varphi_d$  and  $\varphi_r$  should be estimated from the experimental data. These functions were deduced by the procedure described in other works [29, 33] and considering different scenarios and coke gasification with reactions 3, 4 and 5. The scenario that presented the best fit to the experimental data was that in which the reactions 3 and 5 were considered as the coke-forming reactions and the 4 reverse reaction as a reaction that gasifies the coke formed or inhibits its formation. Taking into account the above, the following model was derived for the deactivation functions:

$$\varphi_d = \frac{k_{d1}P_{\text{CH}_4}^2 + k_{d2}P_{\text{H}_2}^2 P_{\text{CO}}^2}{(1 + k_{d3}P_{\text{CO}_2})^2} \quad (11)$$

$$\varphi_r = k_{r1}P_{\text{CO}_2}^2 \quad (12)$$

$k_{d1}$  and  $k_{d2}$  constants result from lumping kinetic constants of elemental steps and equilibrium adsorption constants, while  $k_{d3}$  constant is an equilibrium adsorption constant.

This assumption agrees with the capability of coke removal by  $\text{CO}_2$  at high temperatures [35–37]. These kinetic functions ( $\varphi_d$ ,  $\varphi_r$ ) include the influence of operating conditions on catalyst deactivation.

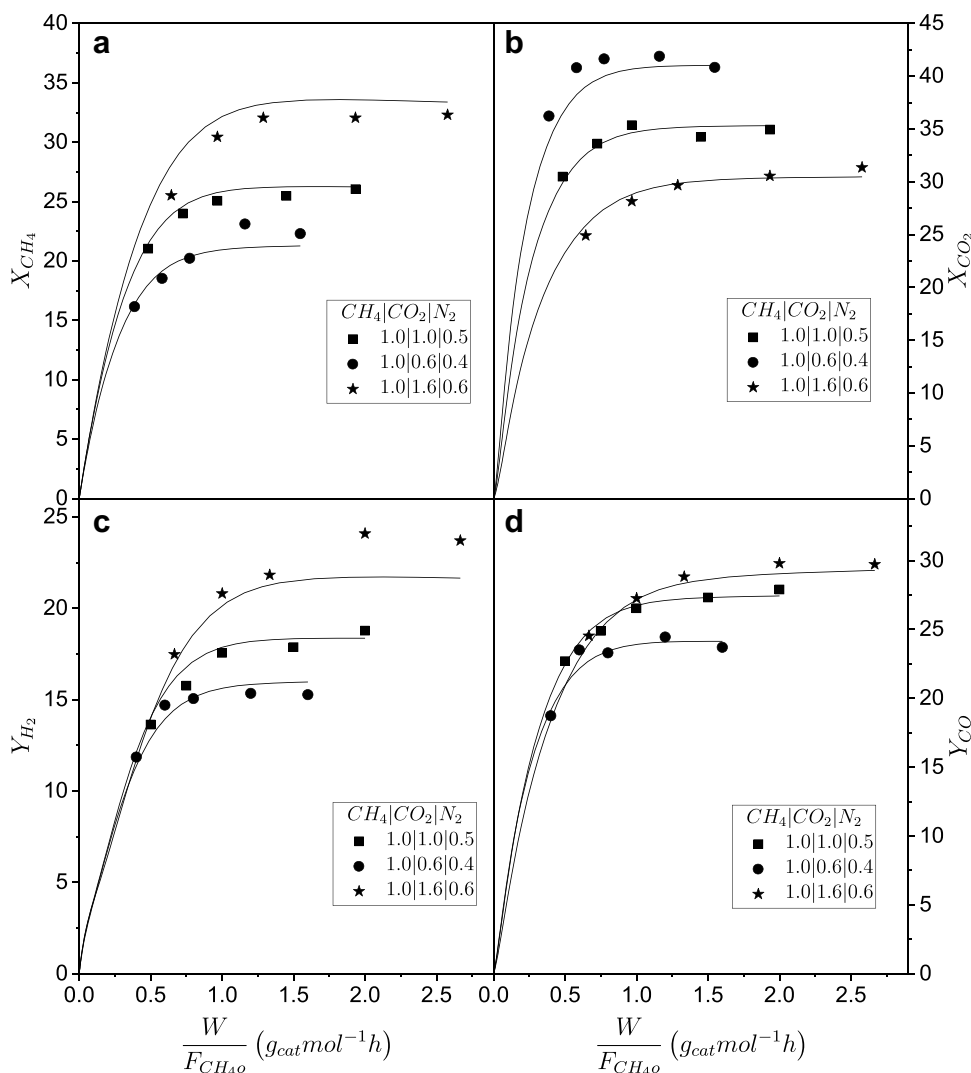
The five deactivation models proposed in Table 3 were considered for deactivation process with  $m=2$  and  $h=1$  or 2. All models exhibited better results when  $h=2$ , which is consistent with the hypothesis of other authors [29]. The goodness of fit and the statistical criteria of model selection are presented in Table 6. The best results were obtained when DMRA 2 equation was employed, so it was incorporated to the total model (Table 7).

A comparison of experimental data and simulations (using the selected total model, Table 7) for the main compounds involved in the process is presented in Fig. 5, for a given temperature and feed composition. A good agreement between experimental and simulated data can be observed.

**Table 5** Comparison of scenarios

Scenarios	R <sup>2</sup>	AR <sup>2</sup>	SSE	AIC	BIC	F	Description
SC1	0.66	0.64	0.042	−1214	−7.95	16,646	r1 + r2
SC2	0.67	0.66	0.040	−1219	−7.99	17,043	r1 + r2
SC3	0.80	0.78	0.028	−1267	−8.30	18,572	r1 + r2 + r3

**Fig. 1** Conversions and yields at different feed compositions. Reaction temperature 525 °C. Experimental data (marker), model data (line)



### 3.3 Relationship Between Catalyst Activity and Coke Concentration

The coke content deposited on the catalyst depends on the reaction conditions such as temperature, time on stream, spatial time and feed composition. The presence of carbon filaments deposited on the catalyst was verified by means of FESEM analysis (Fig. 6).

The effect of feed composition on coke content on the catalyst after a time-on-stream of 4 h at different spatial times is shown in Fig. 7. The coke content was measured during catalyst regeneration by analyzing the gases by gas chromatography.

As can be seen in Fig. 7, the greatest coke content was produced in the experiments with excess of CH<sub>4</sub> in the feed, while less coke deposits were generated with excess of CO<sub>2</sub>. There is a maximum in the coke content with space time, which may be related to the fact that the main reaction (1)

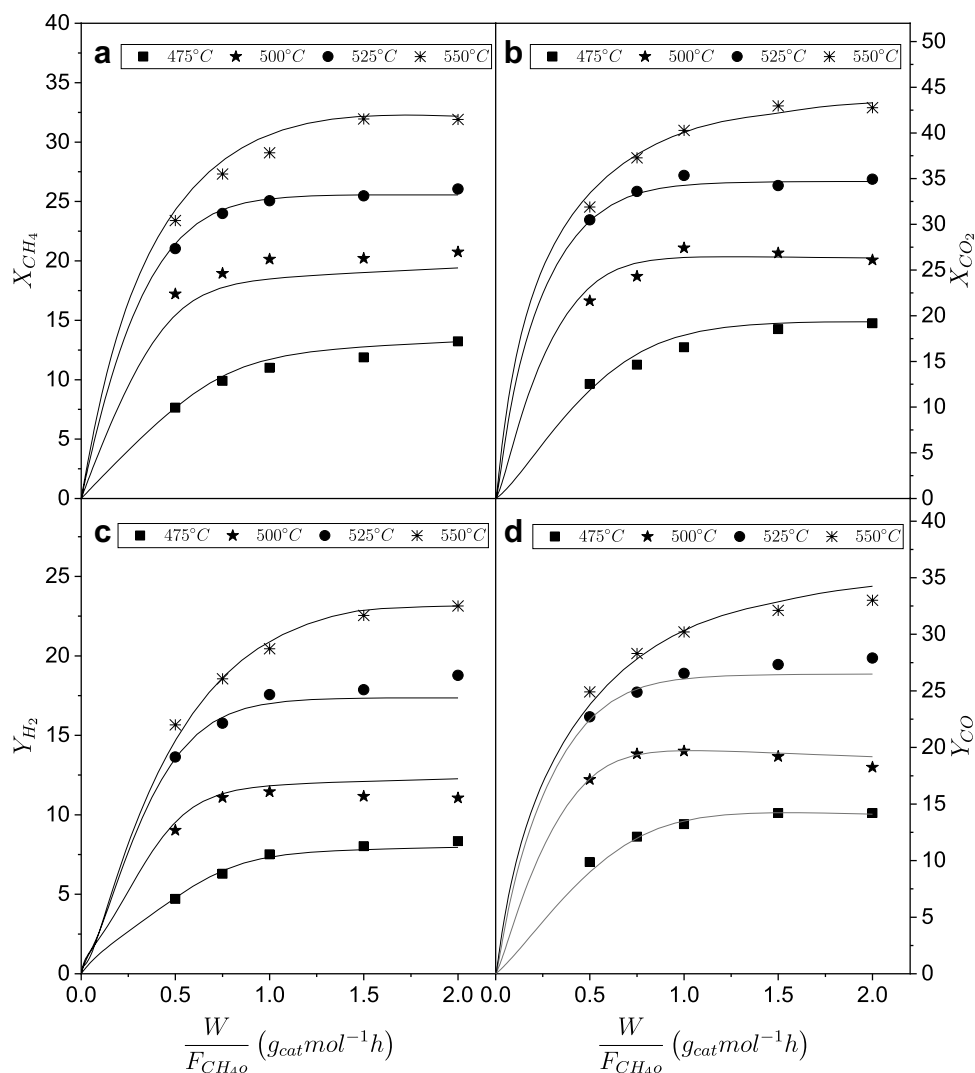
approaches the thermodynamic equilibrium at high space times and the coke formation reactions, i.e. (3) and (5), are less favoured as space time increases and inverse of (4) gains importance.

A relationship between activity and the fraction of active sites occupied by coke was previously given in other works [33, 38]. The value  $m = 2$  was found in the kinetic modelling at zero time. Considering that the fraction of active sites covered by coke is proportional to the coke concentration, the following relationship can be deduced between the activity and the coke content:

$$a = \left(1 - \frac{C_c}{C_{c,max}}\right)^2 \tag{13}$$

where  $C_c$  is coke concentration and  $C_{c,max}$  is maximum coke concentration.

**Fig. 2** Conversions and yields at different reaction temperatures. Molar ratio of the feed  $\text{CH}_4:\text{CO}_2:\text{N}_2=1:1:0.5$ . Experimental data (marker), model data (line)



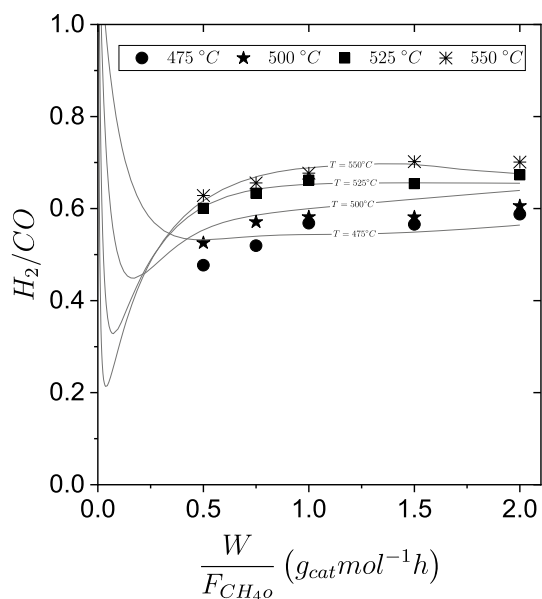
The final activity of the catalyst was calculated ( $t=4$  h) with the activity model DMRA2 previously obtained, and it was related with the coke content experimentally measured for each one of the experiments with different feed compositions. As can be seen in Fig. 7, the effect of spatial time on the coke content is quite complex. Probably there are axial variations of coke content but only the mean value at the end of each experiment was measured. As a simplified approach, an average value of coke concentration was taken for each feed composition and then these values were fitted to the activity model described by Eq. 8.

Figure 8 shows the relationship between calculated activity at the reactor output and coke content in the catalytic bed

for experiments carried out with different feeding conditions. The fitting was made by linearizing Eq. 8. The best fit, with  $R^2=0.93$ , was obtained for a value of  $C_{\text{cmax}}=277.2$  ( $\text{mg}_{\text{coke}}/\text{g}_{\text{catalyst}}$ ). Both activity-coke content and  $C_{\text{cmax}}$  value were incorporated to the total model (Table 7).

### 3.4 Global Fitting

The procedure that has been explained up to now provides a good approach for the equations but it does not take full use of all the experimental data. Therefore, with all the equations obtained, a new fitting was carried out including all experimental data and using the values of



**Fig. 3** Ratio H<sub>2</sub>/CO at different reaction temperatures. Molar ratio of the feed CH<sub>4</sub>:CO<sub>2</sub>:N<sub>2</sub>=1:1:0.5. Experimental data (marker), model data (line)

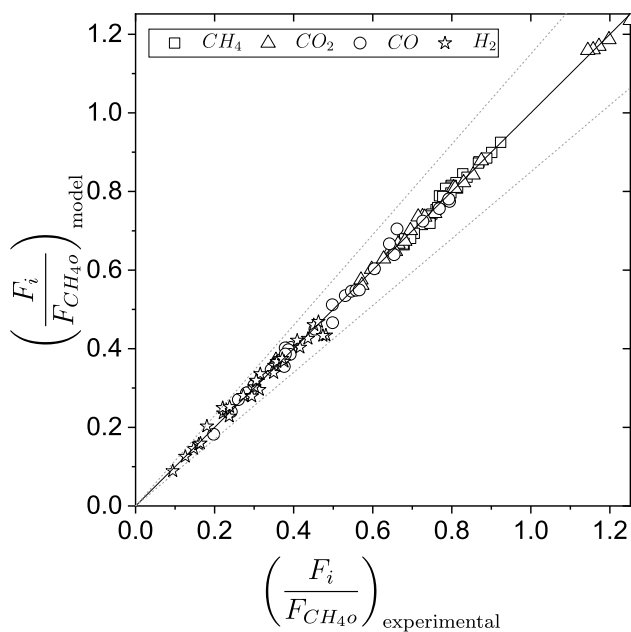


**Fig. 4** Parity plot ( $\pm 15\%$  deviation) for zero-time kinetic modelling.  $F_i = F_{CH_4}, F_{CO_2}, F_{CO}, F_{H_2}$

**Table 6** Deactivation model results

Model	m	h	R <sup>2</sup>	AR <sup>2</sup>	SSE	AIC	BIC	F
LDKM	2	2	0.82	0.82	0.54	-15,972	-8.18	609,642
DMRA 1	2	2	0.83	0.83	0.49	-16,161	-8.28	491,973
DMRA 2	2	2	0.85	0.85	0.44	-16,360	-8.40	527,904
DMRA 3	2	2	0.84	0.84	0.48	-16,207	-8.30	499,628
DMRA 4	2	2	0.82	0.82	0.54	-15,973	-8.18	457,707

**Table 7** Selected models for dry reforming of methane with catalyst deactivation and activity-coke concentration relationship

Id	Model
Zero time	$r_1 = \frac{k_1 K_{CH_4} K_{CO_2} P_{CH_4} P_{CO_2}}{(1 + K_{CH_4} P_{CH_4} + K_{CO_2} P_{CO_2})^2} \left( 1 - \frac{P_{CO}^2 P_{H_2}^2}{P_{CH_4} P_{CO_2} K_{eq1}} \right)$ $r_2 = \frac{k_2 K_{CO_2} K_{H_2} P_{CO_2} P_{H_2}}{(1 + K_{CO_2} P_{CO_2} + K_{H_2} P_{H_2})^2} \left( 1 - \frac{P_{CO} P_{H_2} O}{P_{CO_2} P_{H_2} K_{eq2}} \right)$ $r_3 = \frac{k_3 K_{CH_4} P_{CH_4}}{(1 + K_{CH_4} P_{CH_4} + \frac{P_{H_2}^{1.5}}{K_{H_2}})^2} \left( 1 - \frac{P_{H_2}^2}{P_{CH_4} K_{eq3}} \right)$
Deactivation	$-\frac{da}{dt} = \varphi_d a^{3/2} - \varphi_r a^{1/2}$ $\varphi_d = \frac{k_{d1} P_{CH_4}^2 + k_{d2} P_{H_2}^2 P_{CO}^2}{(1 + k_{d3} P_{CO_2})^2} \varphi_r = k_{r1} P_{CO_2}^2$
Activity-coke concentration	$a = \left( 1 - \frac{C_c}{C_{c,max}} \right)^2 C_{c,max} = 277.2 \left( \frac{mg_{coke}}{g_{catalyst}} \right)$

kinetic constants obtained up to now as initial values. The obtained parity plot is shown in Fig. 9. A good concordance between experimental and simulated data can be observed.

Parameter values with 95% confidence are presented in Table 8. Activation energy for the main reaction (Ea1) is similar to other studies [39].

### 4 Conclusions

A kinetic study, based on a wide experimental program, has been developed for the dry reforming of methane on a Ni–Ce/Al<sub>2</sub>O<sub>3</sub> catalyst. Several scenarios were considered with different sets of reaction in each scenario. The kinetic model that provided the best fit includes the initial reaction rate for the dry reforming, WGSR and methane decomposition reactions. Langmuir–Hinshelwood type models were employed to fit the experimental data. The equations that provided the best fit correspond to a rate determining step with two active sites involved.

In addition, a kinetic model was developed for the catalyst deactivation. Among the models considered, the best fit



**Fig. 5** Exit flow of every specie versus time on stream. Temperature reaction 525 °C and feeding ratio  $\text{CH}_4:\text{CO}_2:\text{N}_2=1:1:0$ . Experimental data (marker), model data (line), space time  $(W/F_{\text{CH}_4} = g_{\text{cat}} \text{ h mol}^{-1})$

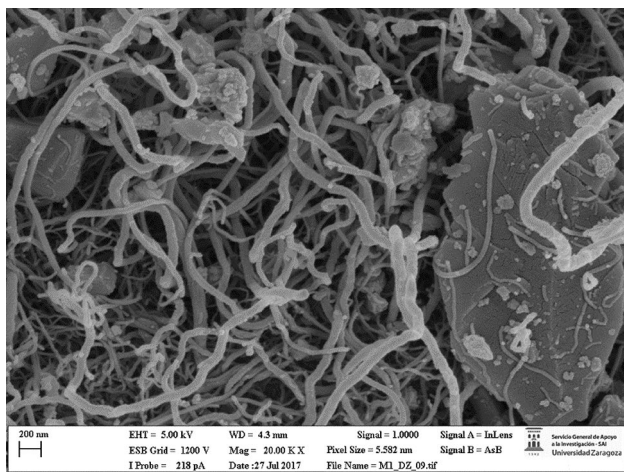
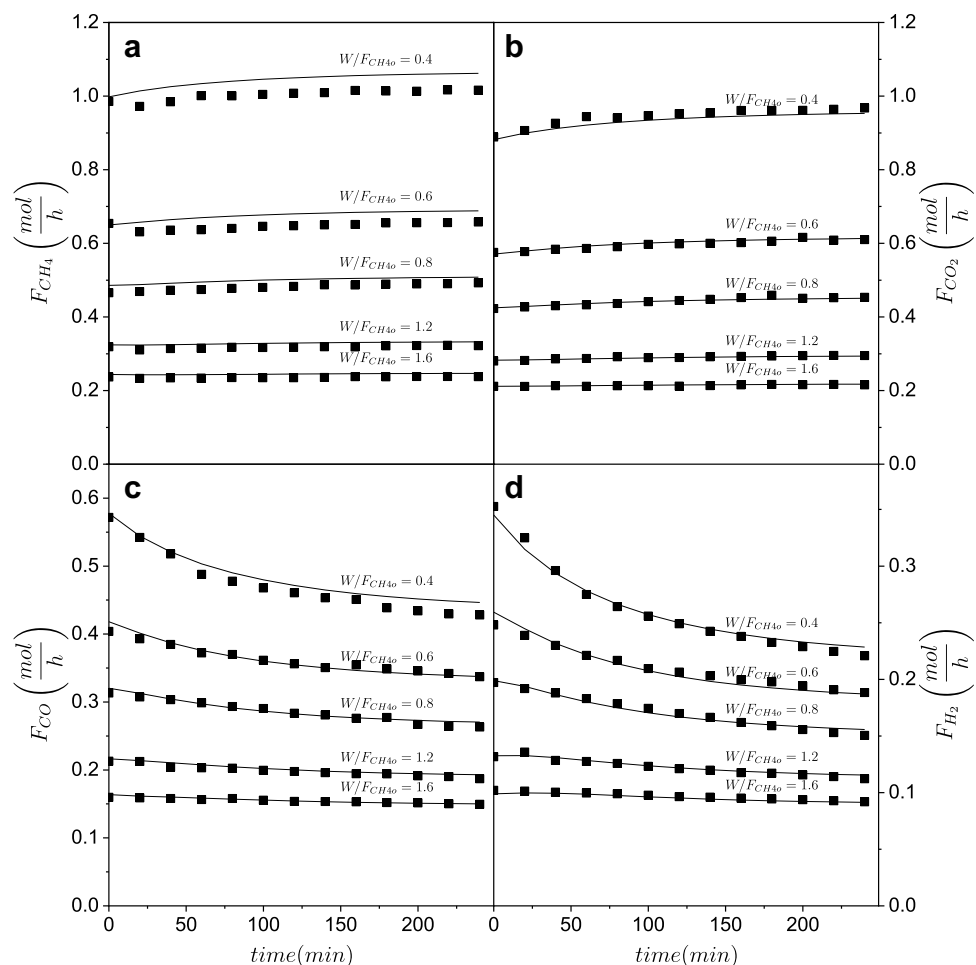


**Fig. 6** FESEM analysis, coke filaments deposited on catalyst. Molar ratio of the feed  $\text{CH}_4:\text{CO}_2:\text{N}_2=1:0.6:0.4$ , reaction temperature  $T=525$  °C, time on stream  $t=4$  h, space time  $W/F_{\text{CH}_4} = 1.6 g_{\text{cat}} \text{ h mol}^{-1}$

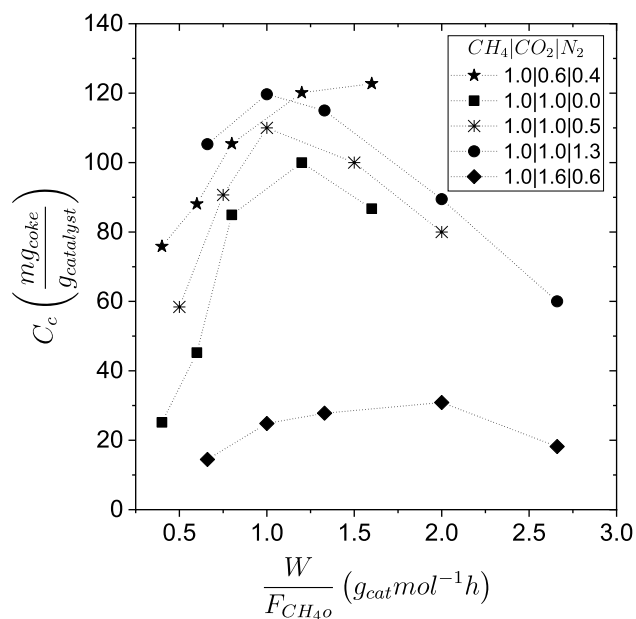


**Fig. 7** Effect of space time on coke deposition for different feeds. Time on stream = 4 h.  $T=525$  °C.  $P=1$  atm

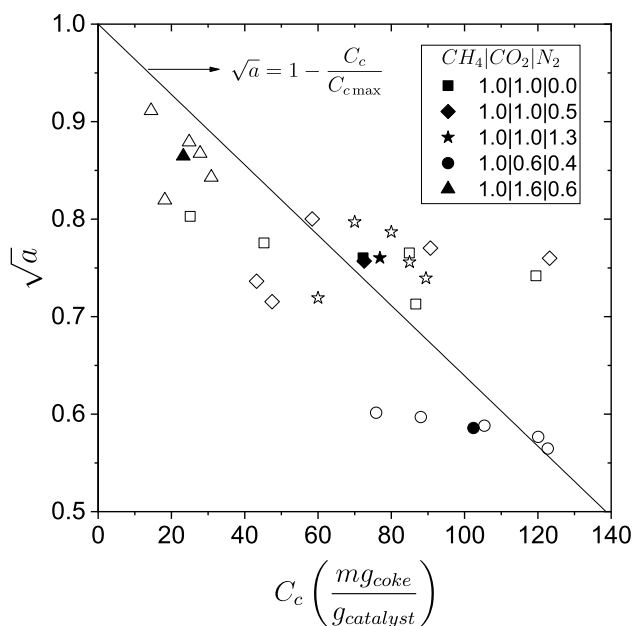


**Fig. 8** Relationship between catalyst activity and deposited coke content (hollow markers represents the experimental values, filled markers represents the experimental average values). Time on stream = 4 h. T = 525 °C. P = 1 atm

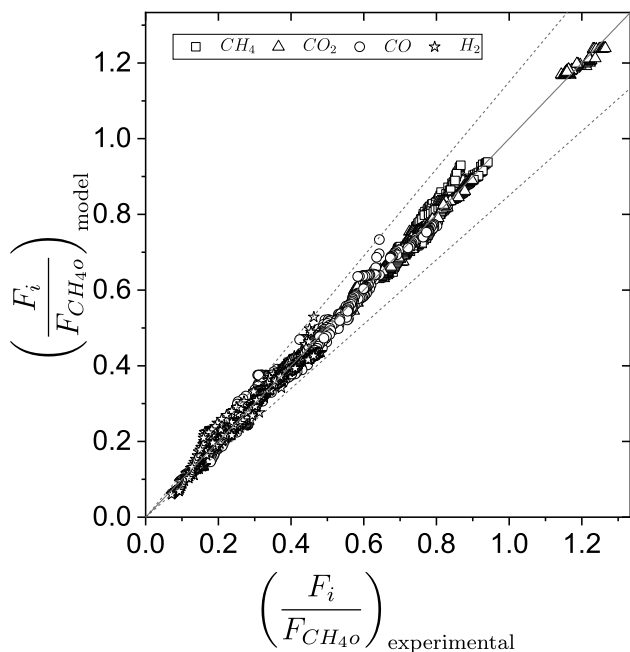


**Fig. 9** Parity plot ( $\pm 15\%$  deviation) for total kinetic modelling (zero-time modelling and catalyst deactivation modelling).  $F_i = F_{CH_4}, F_{CO_2}, F_{CO}, F_{H_2}$

was obtained when a residual activity was included in the model, as a result of the competition between coke formation and coke removal, with two active sites involved in the

**Table 8** Kinetic parameters fitted by selected model

Parameters	Value $\pm$ 95% of confidence	Units
$k_{1o}$	$10.08 \pm 0.21$	$\text{mol g}_{\text{cat}}^{-1} \text{h}^{-1}$
$k_{2o}$	$171.34 \pm 60.8$	$\text{mol g}_{\text{cat}}^{-1} \text{h}^{-1}$
$k_{3o}$	$0.53 \pm 3.15\text{E-}04$	$\text{mol g}_{\text{cat}}^{-1} \text{h}^{-1}$
$K_{CH_4o}$	$3.02 \pm 3.83\text{E-}02$	$\text{bar}^{-1}$
$K_{CO_2o}$	$0.44 \pm 1.21\text{E-}03$	$\text{bar}^{-1}$
$K_{H_2O}$	$16.89 \pm 6.00$	$\text{bar}^{-1}$
$K_{eq1o}$	$5.55\text{E-}03 \pm 3.39\text{E-}04$	$\text{bar}^2$
$K_{eq2o}$	$2.27\text{E-}01 \pm 1.07\text{E-}02$	–
$K_{eq3o}$	$2.63\text{E-}02 \pm 4.32\text{E-}03$	bar
$Ea_1$	$120.88 \pm 0.05$	$\text{kJ mol}^{-1}$
$Ea_2$	$104.38 \pm 1.18$	$\text{kJ mol}^{-1}$
$Ea_3$	$7.37 \pm 0.16$	$\text{kJ mol}^{-1}$
$\Delta H_{CH_4}$	$187.35 \pm 2.37$	$\text{kJ mol}^{-1}$
$\Delta H_{CO_2}$	$21.56 \pm 0.07$	$\text{kJ mol}^{-1}$
$\Delta H_{H_2}$	$51.75 \pm 0.72$	$\text{kJ mol}^{-1}$
$\Delta H_{eq1}$	$265.61 \pm 21.2$	$\text{kJ mol}^{-1}$
$\Delta H_{eq2}$	$38.06 \pm 13.3$	$\text{kJ mol}^{-1}$
$\Delta H_{eq3}$	$144.42 \pm 36.2$	$\text{kJ mol}^{-1}$
$kd_{1o}$	$5.23\text{E-}02 \pm 9.39\text{E-}04$	$\text{min}^{-1} \text{bar}^{-2}$
$kd_{2o}$	$141.49 \pm 3.29$	$\text{min}^{-1} \text{bar}^{-4}$
$kd_{3o}$	$9.07\text{E-}03 \pm 1.64\text{E-}04$	$\text{bar}^{-1}$
$kr_{1o}$	$3.24\text{E-}02 \pm 2.40\text{E-}04$	$\text{min}^{-1} \text{bar}^{-2}$
$\Delta H_{kd1}$	$191.64 \pm 2.70$	$\text{kJ mol}^{-1}$
$\Delta H_{kd2}$	$-398.86 \pm 11.45$	$\text{kJ mol}^{-1}$
$\Delta H_{kd3}$	$792.99 \pm 12.97$	$\text{kJ mol}^{-1}$
$Ea_{kr1}$	$265.89 \pm 1.54$	$\text{kJ mol}^{-1}$

rate determining step of coke formation. Finally, an equation providing the relationship between activity and coke content is proposed.

**Acknowledgements** The authors thank the Ministry of Science and Technology (Spain) for financial support through Project ENE 2013-44350R.

**References**

1. Aramouni NAK, Touma JG, Tarboush BA, Zeaiter J, Ahmad MN (2018) Catalyst design for dry reforming of methane: analysis review. *Renew Sustain Energy Rev* 82:2570–2585
2. Khoshtinat Nikoo M, Amin NAS (2011) Thermodynamic analysis of carbon dioxide reforming of methane in view of solid carbon formation. *Fuel Process Technol* 92:678–691
3. Alenazey FS (2014) Utilizing carbon dioxide as a regenerative agent in methane dry reforming to improve hydrogen production and catalyst activity and longevity. *Int J Hydrog Energy* 39:18632–18641
4. Drif A, Bion N, Brahmi R, Ojala S, Pirault-Roy L, Turpeinen E, Seelam PK, Keiski RL, Epron F (2015) Study of the dry reforming

- of methane and ethanol using Rh catalysts supported on doped alumina. *Appl Catal A* 504:576–584
5. Steinhauer B, Kasireddy MR, Radnik J, Martin A (2009) Development of Ni-Pd bimetallic catalysts for the utilization of carbon dioxide and methane by dry reforming. *Appl Catal A* 366:333–341
  6. Usman M, Wan Daud WMA, Abbas HF (2015) Dry reforming of methane: Influence of process parameters: a review. *Renew Sustain Energy Rev* 45:710–744
  7. Sengupta S, Ray K, Deo G (2014) Effects of modifying Ni/Al<sub>2</sub>O<sub>3</sub> catalyst with cobalt on the reforming of CH<sub>4</sub> with CO<sub>2</sub> and cracking of CH<sub>4</sub> reactions. *Int J Hydrog Energy* 39:11462–11472
  8. Laosiripojana N, Sutthisripok W, Assabumrungrat S (2005) Synthesis gas production from dry reforming of methane over CeO<sub>2</sub> doped Ni/Al<sub>2</sub>O<sub>3</sub>: influence of the doping ceria on the resistance toward carbon formation. *Chem Eng J* 112:13–22
  9. Ay H, Üner D (2015) Dry reforming of methane over CeO<sub>2</sub> supported Ni, Co and Ni-Co catalysts. *Appl Catal B* 179:128–138
  10. Herguido J, Menéndez M (2017) Advances and trends in two-zone fluidized-bed reactors. *Curr Opin Chem Eng* 17:15–21
  11. El Solh T, Jarosch K, de Lasa H (2003) Catalytic dry reforming of methane in a CREC riser simulator kinetic modeling and model discrimination. *Ind Eng Chem Res* 42:2507–2515
  12. Gokon N, Yamawaki Y, Nakazawa D, Kodama T (2011) Kinetics of methane reforming over Ru/ $\gamma$ -Al<sub>2</sub>O<sub>3</sub>-catalyzed metallic foam at 650–900 °C for solar receiver-absorbers. *Int J Hydrog Energy* 36:203–215
  13. Kathiraser Y, Oemar U, Saw ET, Li Z, Kawi S (2015) Kinetic and mechanistic aspects for CO<sub>2</sub> reforming of methane over Ni based catalysts. *Chem Eng J* 278:62–78
  14. Mark MF, Maier WF, Mark F (1997) Reaction kinetics of the CO<sub>2</sub> reforming of methane. *Chem Eng Technol* 20(6):361–370
  15. Benguerba Y, Virginie M, Dumas C, Ernst B (2017) Methane dry reforming over Ni-Co/Al<sub>2</sub>O<sub>3</sub>: kinetic modelling in a catalytic fixed-bed reactor. *Int J Chem React Eng* 15(6)
  16. Özkara-Aydinoğlu Ş, Erhan Aksoylu A (2013) A comparative study on the kinetics of carbon dioxide reforming of methane over Pt–Ni/Al<sub>2</sub>O<sub>3</sub> catalyst: effect of Pt/Ni ratio. *Chem Eng J* 215–216:542–549
  17. Wang S, Lu GQ (1999) A comprehensive study on carbon dioxide reforming of methane over Ni/ $\gamma$ -Al<sub>2</sub>O<sub>3</sub> catalysts. *Ind Eng Chem Res* 38(7):2615–2625
  18. Pakhare D, Spivey J (2014) A review of dry (CO<sub>2</sub>) reforming of methane over noble metal catalysts. *Chem Soc Rev* 43:7813–7837
  19. Ginsburg JM, Piña J, El Solh T, de Lasa H (2005) Coke formation over a nickel catalyst under methane dry reforming conditions: thermodynamic and kinetic models. *Ind Eng Chem Res* 44(14):4846–4854
  20. Ayodele BV, Khan MR, Lam SS, Cheng CK (2016) Production of CO-rich hydrogen from methane dry reforming over lanthania-supported cobalt catalyst: kinetic and mechanistic studies. *Int J Hydrog Energy* 41(8):4603–4615
  21. Wang S, Lu GQ, Millar GJ (1996) Carbon dioxide reforming of methane to produce synthesis gas over metal-supported catalysts: state of the art. *Energy Fuel* 10:896–904
  22. Wang S, Lu GQ (2000) Reaction kinetics and deactivation of Ni-based catalysts in CO<sub>2</sub> reforming of methane. *React Eng Pollut Prev* 8:75–84
  23. Osaki T, Horiuchi T, Suzuki K, Mori T (1997) Catalyst performance of MoS<sub>2</sub> and WS<sub>2</sub> for the CO<sub>2</sub>-reforming of CH<sub>4</sub> suppression of carbon deposition. *Appl Catal A* 155(2):229–238
  24. Foo SY, Cheng K, Nguyen TH, Adesina AA (2010) Kinetic study of methane CO<sub>2</sub> reforming on Co–Ni/Al<sub>2</sub>O<sub>3</sub> and Ce–Co–Ni/Al<sub>2</sub>O<sub>3</sub> catalysts. *Catal Today* 164:221–226
  25. Barroso Quiroga MM, Castro Luna AE (2007) Kinetic analysis of rate data for dry reforming of methane. *Ind Eng Chem Res* 46:5265–5270
  26. Fan MS, Abdullah AZ, Bhatia S (2009) Catalytic technology for carbon dioxide reforming of methane to synthesis gas. *Chem Cat Chem* 1:192–208
  27. Benguerba Y, Dehimi L, Virginie M, Dumas C, Ernst B (2015) Modelling of methane dry reforming over Ni/Al<sub>2</sub>O<sub>3</sub> catalyst in a fixed-bed catalytic reactor. *React Kinet Mech Catal* 114:109–119
  28. Richardson JT, Paripatyadar SA (1990) Carbon dioxide reforming of methane with supported rhodium. *Appl Catal* 61:293–309
  29. Snoeck JW, Froment GF, Fowles M (1997) Kinetic study of the carbon filament formation by methane cracking on a nickel catalyst. *J Catal* 169:250–262
  30. Snoeck JW, Froment GF, Fowles M (2002) Steam/CO<sub>2</sub> reforming of methane. Carbon filament formation by the Boudouard reaction and gasification by CO<sub>2</sub>, by H<sub>2</sub>, and by steam: kinetic study. *Ind Eng Chem Res* 41:4252–4265
  31. Chein RY, Hsu WH, Yu CT (2017) Parametric study of catalytic dry reforming of methane for syngas production at elevated pressures. *Int J Hydrog Energy* 42:14485–14500
  32. Monzón A, Romeo E, Borgna A (2003) Relationship between the kinetic parameters of different catalyst deactivation models. *Chem Eng J* 94(1):19–28
  33. Corella J, Adanez J, Monzón A (1988) Some intrinsic kinetic equations and deactivation mechanisms leading to deactivation curves with a residual activity. *Ind Eng Chem Res* 27:375–381
  34. Świrk K, Gálvez ME, Motak M, Grzybek T, Da Costa P (2018) Syngas production from dry methane reforming over yttrium-promoted nickel-KIT-6 catalysts. *Int J Hydrog Energy* 44(1):274–286
  35. Gimeno MP, Soler J, Herguido J, Menéndez M (2010) Counteracting catalyst deactivation in methane aromatization with a two zone fluidized bed reactor. *Ind Eng Chem Res* 49:996–1000
  36. Yus M, Soler J, Herguido J, Menéndez M (2018) Glycerol steam reforming with low steam/glycerol ratio in a two-zone fluidized bed reactor. *Catal Today* 299:317–327
  37. Ugarte P, Durán P, Lasobras J, Soler J, Menéndez M, Herguido J (2017) Dry reforming of biogas in fluidized bed: process intensification. *Int J Hydrog Energy* 42:13589–13597
  38. Corella J, Asúa JM (1982) Kinetic equations of mechanistic type with nonseparable variables for catalyst deactivation by coke. Models and data analysis methods. *Ind Eng Chem Process Des Dev* 21:55–61
  39. Chen D, Lødeng R, Anundskås A, Olsvik O, Holmen A (2001) Deactivation during carbon dioxide reforming of methane over Ni catalyst: microkinetic analysis. *Chem Eng Sci* 56:1371–1379

**Publisher's Note** Springer Nature remains neutral with regard to jurisdictional claims in published maps and institutional affiliations.